Petruzzelli F., Della Corte G., Iervolino I. (2012) Seismic Risk Assessment of an Industrial Steel Building Part 1: Modelling and Analysis. Proc of. 15WCEE, Lisboa, PT. Paper No. 3086.

Seismic Risk Assessment of an Industrial Steel Building Part 1: Modelling and Analysis

F. Petruzzelli, G. Della Corte & I. Iervolino
Università degli Studi di Napoli Federico II, Italy

SUMMARY:
In this paper seismic modelling and analysis of an existing steel industrial building are described. The building is made of different portions built between 1970s and 1990s and it is located in central Italy. The study addresses some issues which emerged to be important in order to evaluate seismic performances: (i) modelling of column base connections, which in case of existing structures may be significantly different from the standardized detailing for which structural codes give information; (ii) the role and effect of transverse bracing between parallel bi-dimensional frames, which is investigated by comparing three-dimensional and bi-dimensional models; (iii) the role of P-Delta effects and the assessment of sidesway global collapse; (iv) the importance to check the structure for local failure modes involving roof members and connections. Results from nonlinear static and dynamic analysis, both in terms of global drift and member force demand, are presented and discussed.

Keywords: Connections, Demand, Capacity, Existing structures.

1. INTRODUCTION

The industrial building stock of many countries is significantly contributed by steel buildings. Although these structures are generally relatively lightweight and, in most of cases, designed for wind actions, the assessment of their seismic performance is important for the estimation of the possible consequences of earthquakes, in terms of direct damage and/or business interruption. The seismic analysis of existing industrial steel structures presents some peculiar modelling aspects which have been subject of relatively little investigation with respect to other types of existing structures. One frequent type of damage observed in past earthquakes is brace buckling (e.g Ozakgul *et al.*, 2011). Specific research efforts have been addressed to investigate the role and the modelling of roof panels (De Matteis *et al.*, 1999; Mastrogiuseppe *et al.*, 2008). An investigation of the seismic response of an existing industrial steel building is presented in the following. Starting from as-built data collection, the study has been addressed to develop the complete process of seismic risk assessment, through the use of current performance-based analysis methods. The study is summarised in two companion papers: this one is focused on the main modelling aspects and results from analysis of seismic performance; the companion paper (Petruzzelli *et al.*, 2012) illustrates the fragility derivation and, upon integration with site-specific hazard, the structural risk assessment, that is, probability of failures.

2. THE BUILDING

An aerial view of the building under investigation is shown in Figure 1*a*. The building consists of four different parts, built in different years and separated by (insufficient seismically) joints, as shown in Figure 1*b*. In particular, the white-shaded area in Figure 1*b*, refers to the most ancient structure, built in 1971 and separated into two portions by a longitudinal joint parallel to the *x*-direction. In 1979 these two portions were enlarged with no separation between the new and old constructions (light grey-shaded area in Figure 1*b*). Considering that the enlargements were done using the same materials and structural dimensions as those of the previous 1971 structures, in the following, we will refer to these parts of the building as “1971/79” structures. Finally, the most recent parts were built in 1991, as

indicated by the dark grey shadow in Figure 1*b*. The overall plan dimensions are 252 m x 192 m (Fig. 1*b*). It is worth noting that, both building were designed according to obsolete seismic codes, with significant underestimation of design seismic intensities.

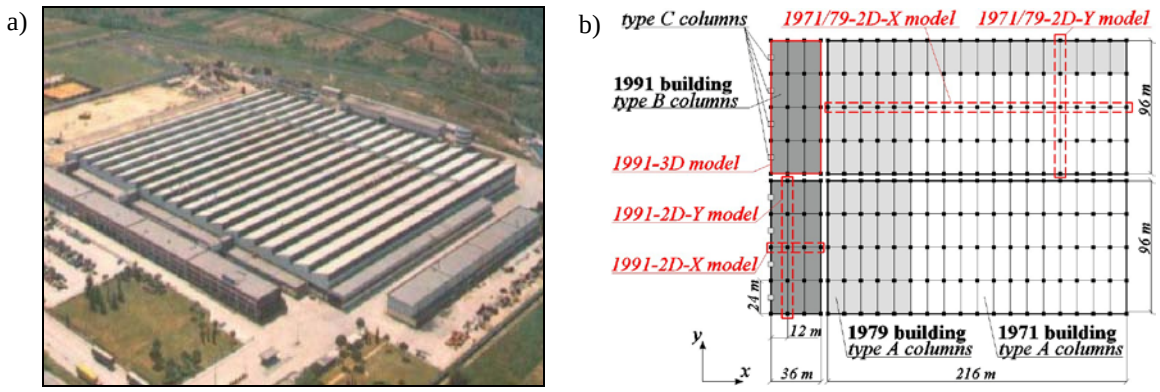

Figure 1. (a) Aerial view and (b) schematic drawing illustrating different portions of the building.

Parts made in different years present the same structural plan layout (12 m x 24 m) and a similar roof structure. The latter is made with shed-type trusses in the *x*-direction and Pratt trusses in the *y*-direction. Single-bay structural cross sections of trusses in *x*- and *y*-direction, as given in the original design drawings, are shown in Figure 2. The roof structure is completed by *x*-shaped bracing, and minor elements supporting the closure panels.

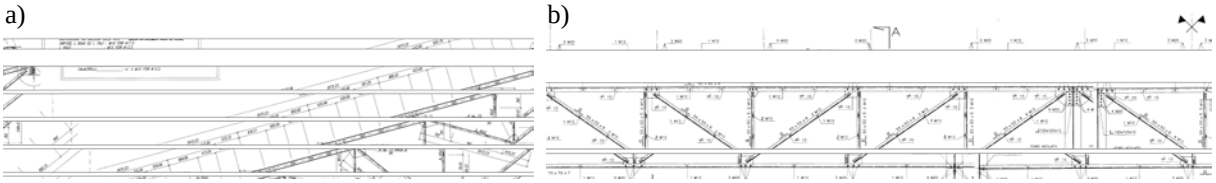

Figure 2. Single-bay structural cross-sections of trusses in *x*- (a) and *y*-direction (b).

Vertical resisting members, sustaining the roof structure and ensuring resistance to lateral loading, are composite battened columns. In the portions of the structure built in 1971/79, composite columns are made of two IPE 360 shapes, reinforced on the flanges with 15 mm thick plates, coupled together by battens consisting of plates welded to the flanges (Fig. 3*a*). A HE A 240 profile is welded at the top-end of the column (+7.825 m) in order to connect the column to the roof trusses. These composite columns will be hereafter referred to as columns of type A, whose plan location is also indicated in Figure 1*b*. In the portions built in 1991, the main columns, indicated as type-B (Fig. 1*b*), are also composite members, obtained by battening of IPE 600 shapes. Battens of type-B columns are obtained by cutting pieces from hot-rolled profiles with HE A 500 cross-section and bolting their flanges to the web of the main column members, as shown in Figure 3*b*. A hot-rolled HE A 400 shape is placed at the top-end of the column, connecting the latter to the roof structure. Flanges of the HE A 400 shape are connected to the web of the composite column members by means of bolts, as made for battens (Fig. 3*c*). In addition to the above, there are also columns (type-C) consisting of a single hot-rolled HE A 340 shape (Fig. 3*d*), located at the left-hand side perimeter frame shown in Figure 1*b*. Figure 3 also shows the detail of the connections to the foundation for different types of columns. For type A columns, the connection is provided by a single 20 mm thick steel plate, anchored by bolts to the RC foundation (Fig. 3*a*). For type B columns, the connection is constituted of two separate 30 mm thick steel base plates, each one anchored to the foundation by means of three bolts (Fig. 3*b*). The connection of type-C columns to the foundation, similarly to other types, is made by a steel plate and anchor bolts (Fig. 3*d*). In each of the cases described above, stiffening plates with thickness varying between 15 and 20 mm are welded to the vertical members.

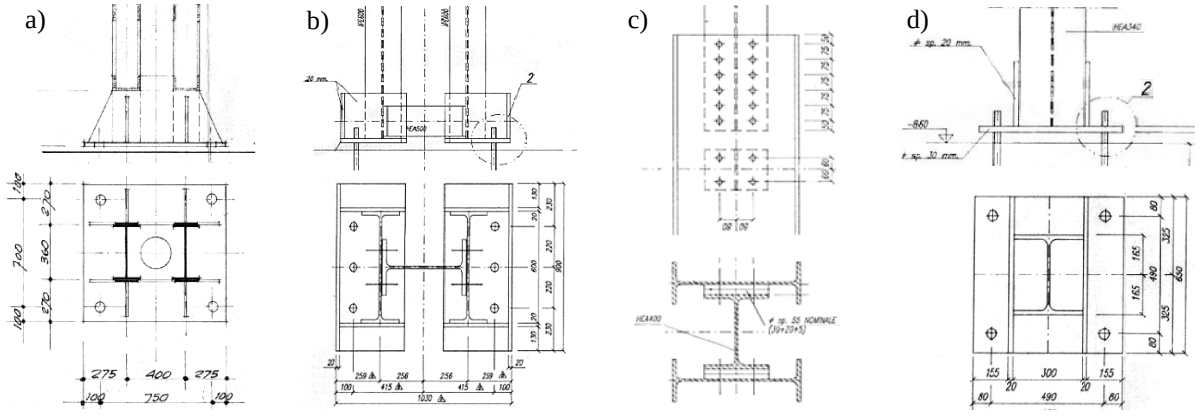

Figure 3. Original design drawings: (a) type-A columns, (b) type-B columns, (c) detail of top of type-B columns, (d) type-C columns.

3. STRUCTURAL MODELLING

3.1. General

Based on both original design drawings and visual on-site inspections of the facility, it was possible to characterize the structural geometry. For the purposes of this study, characteristic values of the material properties are assumed to be those indicated by original design drawings. Accordingly, any structural member is assumed to be characterised by a yield stress f_y = 235 MPa, while f_y = 275 MPa is used for column base plates and f_y = 355 MPa is used for roof member gusset plate connections. Bolts are of grade 8.8 and the concrete used for foundation structures is assumed to be C20/25 grade (CEN, 2005). Virtually, non-linear behaviour of the structure derive from: 1) bracing elements connecting parallel frames; 2) members and connections of the main roof trusses; 3) top cross-sections of columns; 4) column base connections; 5) battens and relevant connections to column members.
The bracing elements connecting parallel frames (bullet 1 of the previous list) are characterized by high slenderness, leading to early buckling for low levels of seismic intensity. To account for this phenomenon, referring to the portion of more recent construction, two structural models were analysed: a three-dimensional model, hereafter referred to as "1991-3D" model (Fig. 4*a*), and two two-dimensional models, a "1991-2D-Y" model of a frame in the *y*-direction (Fig.4*b*) and a "1991-2D-X" model of a frame the *x*-direction (Fig.4*c*).

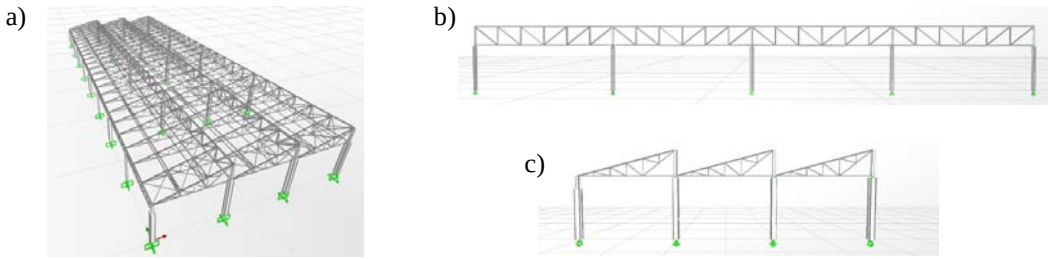

Figure 4. Structural models for 1991 portion: (a) “1991-3D”, (b) “1991-2D-Y” and (c) “1991-2D-X” model.

In the three-dimensional model all the structural elements are considered, including the bracing elements but the latter are assumed to behave elastically. The two-dimensional models are obtained extracting two single frames from the structure, each one subjected to vertical loads derived from a tributary area criterion. Analysis of response of the 3D model with elastic braces and of the 2D frame model allows identifying boundaries to the real structural response, which is expected to be intermediate to the above two limit cases because of early brace buckling and consequent degradation of the coupling effect. Only bi-dimensional models have been analysed for the 1971/79 building, indicated hereafter as "1971/79-2D-Y" and "1971/79-2D-X". With reference to the possible failure of

roof members and/or connections (point 2 of the previous list), it should be noted that, because of the lack in structural redundancy, this failure will transform the statically determined roof structure into a mechanism. A sample case of roof collapse due to connection failure is described by Brencich (2010). Also in consideration of the reduced ductility capacity of such failure modes, they have been treated as "brittle" elements. Therefore, their nonlinear response was not explicitly included in the structural model, but their force demand-to-capacity ratio has been checked after the analysis. The third and fourth sources of inelasticity, the column top cross sections and their base-plate connections, have been explicitly incorporated in the seismic demand analysis. Finally it was checked that the battens are able to sustain the maximum internal action corresponding to the peak column shear force associated with flexural yielding at the top and bottom ends. Lumped plasticity finite element models have been analysed by means of SAP 2000 v.14 software (Wilson, 2002), assuming an equivalent viscous damping ratio equal to 2% of the critical value and taking into account P-Delta effects. Column plastic hinges located at the top end cross sections, immediately below the roof trusses, have been modelled as bilinear, with 3% post-yield stiffness ratio. Modelling of column base connections is discussed at Section 3.2. Account was taken of the increase of the composite column deformability, by modifying the shear deformability according to Eurocode 3 (EC3; CEN, 2005). The ground motions, used in the nonlinear dynamic analysis described in the following Sections, have been selected based on a seismic hazard assessment described in the companion paper (Petruzzelli *et al.*, 2012).

3.2. Modelling column base connections

3.2.1. Type C column base connections

Type C column base connections (Fig. 3*d*) represent a design solution widely used in the professional practice. As it can be observed from Figure 3*d*, the stiffening plates make such a connection slightly different from the standard type presented in EC3. Moreover, since EC3 is dedicated to analysis under static loads, it gives information as to how calculate the flexural strength for a given eccentricity of the axial force ($e_d = M_{Ed} / N_{Ed}$). However, in the case of seismic action, it is reasonable to assume that the axial force remains constant or slightly variable with respect to the value produced by the seismic combination of gravitational loads ($N_{G,s}$), while the bending moment will grow significantly due to horizontal seismic forces. To take account of this aspect, the maximum value e_{max} of the eccentricity that the connection may sustain (i.e., the eccentricity that produces the failure of the weakest component) is determined first. Given the symmetry of the connection, the possible limit equilibrium conditions are shown in Figure 5.

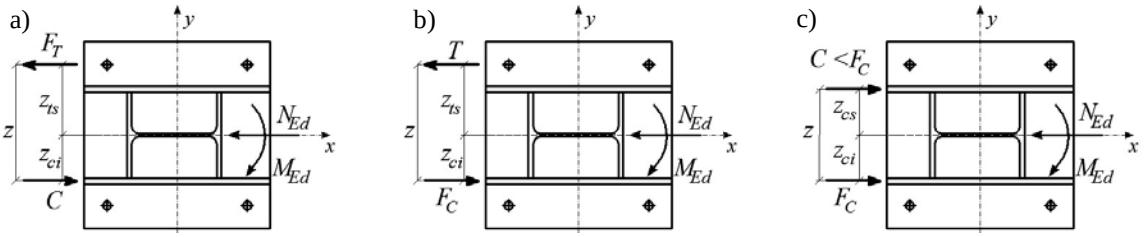

Figure 5. Limit equilibrium conditions: "large" eccentricity and tension failure (a); "large" eccentricity and compression failure (b); "small" eccentricity and compression failure.

In particular, panels <u>*a*</u> and *b* of Figure 5 are related to the case of "large eccentricity", where the acting axial force is placed outside the base plate portion enclosed between the two stiffening plates and the failure may be due to excessive tension (*a*) or excessive compression (*b*). Panel c of Figure 5 represents the case of "small eccentricity," in which the connection is fully compressed. Using formulations of EC3, the bending strength corresponding to each failure mode can be computed, for varying axial forces. The flexural capacity of the connection is provided by the smallest value of bending moment M_{Rd}, corresponding to the acting axial force $N_{G,s}$. Once the maximum eccentricity, $e_{max}=M_{Rd} / N_{G,s}$, has been calculated, the moment-rotation relationship can be obtained for any given value of the eccentricity in the range (0, e_{max}). The first derivative of the moment-rotation relationship for the real loading conditions (varying bending moment with constant axial force) is then considered

to be equal to the derivative of the moment-rotation relationship obtained for the given value of the eccentricity e^*. Henceforth, the moment-rotation response of the connection for a varying eccentricity can be obtained. An example of this calculation procedure is shown in Figure 6, with reference to type-C columns. In Figure 6*a* the moment-rotation response of the connection for any given value of the eccentricity in the range (0, e_{max}) is shown. In Figure 6*b* the resulting moment-rotation response for varying eccentricity is illustrated, together with limiting values of rotational stiffness and strength, as given by EC3 for classifying a connection. It can be seen that the specific connection is rigid and partial strength.

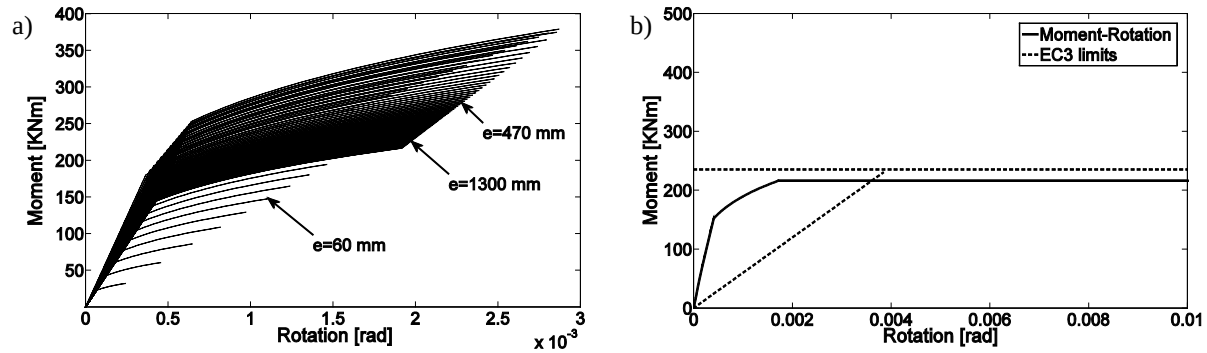

Figure 6. Moment-rotation relationships: (a) for fixed values of axial force eccentricity and (b) for varying (increasing) values of eccentricity (lateral loading with a constant axial force).

3.2.2. Types A and B column base connections

Type B column base connections are significantly different from the standard type covered by EC3. A decomposition of the total connection response into individual contributions is then pursued (Fig. 7).

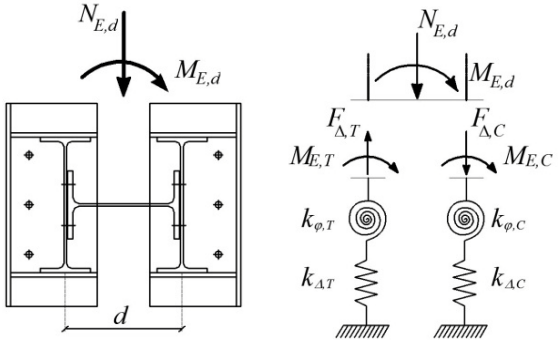

Figure 7. Decomposition of connection response into separate contributions.

The total bending moment and axial force acting at the base of the composite column is decomposed into contributions due to single column members and transmitted to the corresponding base plate. Two springs are used to characterize each base plate connection, one for translations and one for rotations. Taking into account the overall symmetry of the connection formed by the two plates, the total rotational stiffness is obtained by assembling the individual contributions, according to the following equation (Eqn. 3.1).

$$k_{\varphi}^{tot} = k_{\Delta,C} \cdot \frac{d}{2} + k_{\Delta,T} \cdot \frac{d}{2} + k_{\varphi,C} + k_{\varphi,T} \tag{3.1}$$

The individual spring stiffness has been calculated on the basis of the schemes illustrated in Figure 8. Panels *a b* of Figure 8 show the schemes for the evaluation of the translational stiffness of the springs in compression ($k_{\Delta,C}$) and tension ($k_{\Delta,T}$), respectively. Similarly, Panels *c* and *d* are related to the determination of the rotational stiffness of the individual base plates, for the two opposite bending

directions ($k_{\varphi,C}$ and $k_{\varphi,T}$). Figure 9*a* shows the resulting moment-rotation curve, obtained for type B columns. It can be seen that the connection is semi-rigid and partial strength. Figure 9*b* shows the moment-rotation relationship for type A column, obtained with the same method discussed for type C column base connections. The connection results to be semi-rigid and partial strength.

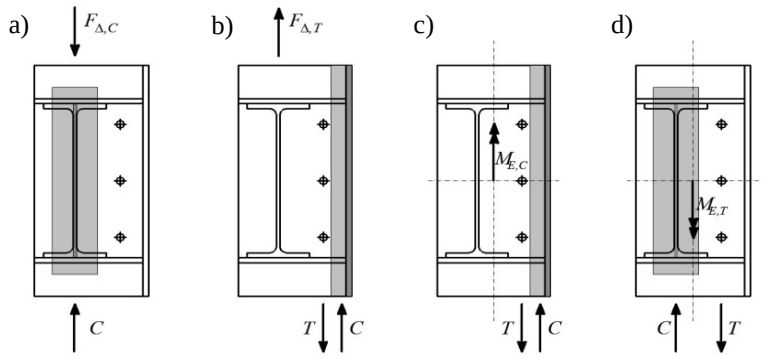

Figure 8. Individual contributions to connection response.

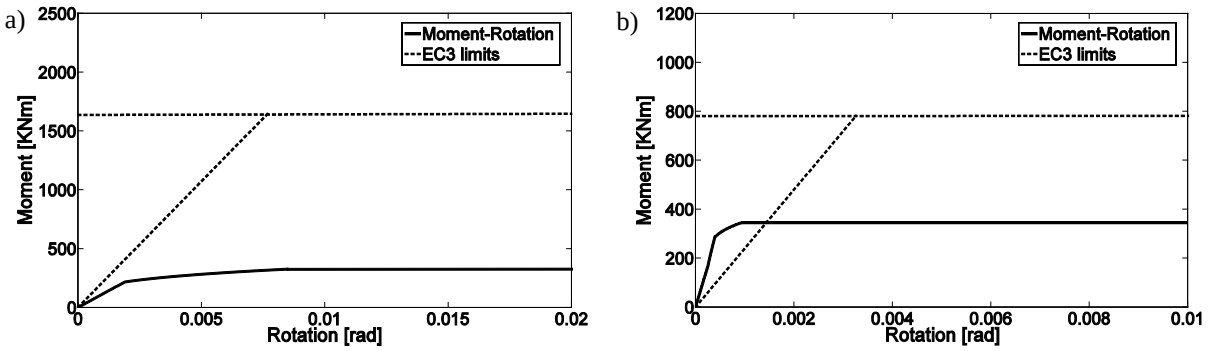

Figure 9. Moment-rotation relationships: (a) type B and (b) type A columns.

3.2.3. Hysteresis models

Modelling accurately the hysteretic response of column base connections was out of the scope of this study, which was rather addressed to investigate more general modelling issues. Therefore, neither experimental nor analytical efforts were made in order to characterise such hysteresis behaviour. The cyclic moment-rotation response of column base connections was approximated by the Pivot hysteresis model (Dowell *et al.*, 1998) without including any stiffness or strength degradation. Flexural plastic hinges in hot rolled steel members were approximated by a stable bilinear moment-rotation response. Neglecting degradation is known to be a reliable approximation for high levels of structural performance, but it may result in poor approximations in case of a collapse limit state (Della Corte *et al.*, 2002; Ibarra *et al.*, 2005). However, the effect of strength deterioration at low performance levels has been considered in some indirect way, by assuming conservative values of the drift capacity at collapse, as discussed in Section 4.2.

4. ANALYSIS AND RESULTS

4.1. Non-linear static analyses

Static pushover analyses (SPO) were carried out under displacement control, assuming a control node located at the center of gravity of the model, at a height equal to the top of composite columns. The adopted lateral load pattern is proportional to the first modal shape in the considered direction, and kept constant during the analysis. Results are represented in terms of both dimensional and normalised pushover response curves. The dimensional representation typically plots the base shear force versus

control node displacement relationship; the normalised representation, plots the base shear divided by the structure weight and first mode participating factor versus the control node displacement divided by the column height. The normalised representation allows a more direct comparison between different structures in terms of initial stiffness and peak strength. Figure 10 shows SPO curves for all the examined structural models. Considering the response of the "1991-3D" model a gradual nonlinearity in the pushover curve can be observed. This is due to the yielding of some frames before others because of some eccentricity between the center of mass and the center of stiffness.

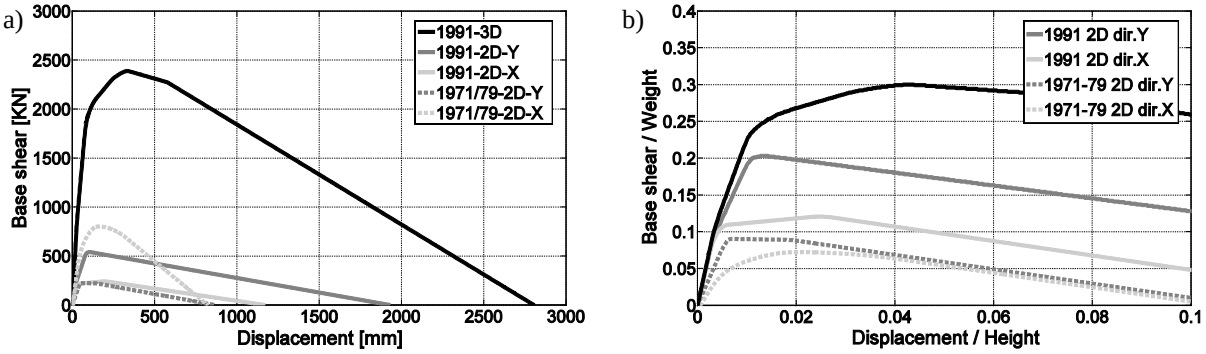

Figure 10. Pushover response of all considered structures: (a) dimensional and (b) normalised curves.

Looking at Figure 10*b*, it can be noticed that the "1991" structures are characterised by an elastic stiffness and a normalised strength higher than those of the "1971/79" structures. However, from Figure 10*a*, it can be observed that the "1991" structures show ultimate displacements (those corresponding to zero base shear) larger than those characterising the "1971/79" structures. Moreover, the post peak slope of the dimensional pushover curves for the "1991" models are lower than those obtained for the "1971/79" models. These observations can lead to the following considerations: "1971/79" building, as consequence of a larger elastic period with respect to the one of "1991" portion (about 1.6 s versus 0.98 s) is expected to show larger displacement demands, while the building response remains stable in the plastic range. At large displacement demand, P-Delta effects take a significant role, and they have a more pronounced influence on the "1971/79" building than they have on the "1991" building frame. Consequently, for increasing levels of earthquake intensity (spectral acceleration), the rate of increase in the drift demand to the "1971/79" building is expected to be larger than the rate for the "1991" building. This behaviour will reasonably lead to a number of ground motion records producing collapse of the "1971/79" building frame larger than that for the "1991" building frame. Moreover, considering the two different directions of a given portion of the building, from the aforementioned consideration about initial stiffness, normalised strength and post-peak slope, the *x*-direction seems to be the most dangerous for both buildings, so that larger seismic demands are expected for these frames.

4.2. Non-linear dynamic analyses

The IDA method (Vamvatsikos and Cornell, 2002) was implemented in this study. Results are summarized in the following in the form of plots showing the relationship between the assumed earthquake intensity measure (i.e., spectral acceleration at the fundamental period of each structure) and the selected engineering demand parameter (EDP). The EDP will be either a displacement or force quantity. Peak transient roof drift ratios as well as peak positive and negative force demand to members and connections will be considered. The set of acceleration records employed in the analyses is obtained from a procedure described in the companion paper (Petruzzelli *et al.*, 2012). It is known that, when a sufficiently large ground motion intensity is used, the structural response from numerical analyses either unreliable/ unavailable as a consequence of convergence issue of the structural analysis software. These situations can be referred to as dynamic or numerical instabilities. These two cases have been treated in the same way, i.e. assuming that they both correspond to sidesway collapse of the structure. The limiting value of drift used to distinguish collapse cases from non-collapse ones has been obtained starting from the value corresponding to a zero lateral strength on the pushover response

curves (Fig. 10*a*). This zero-strength drift has been multiplied by an empirical but arbitrary reduction factor of 0.5, which is introduced to take into account possible degradation of plastic zones occurring at large values of the drift ratio. Drift values larger than this limit will be treated separately to evaluate the probability of collapse. The collapse limit is shown in the following Figures 11, 12 and 13 by a vertical dashed line with a symbol δ_U.

4.2.1. Global seismic demand and capacity (drift)

Figures 11 to 13 show results of IDA in terms of global peak transient drift ratios. According to the FEMA 356 provisions (ASCE, 2000), the drift capacity in the case of existing steel buildings can be set equal to δ_{IO} = 0.0075 rad, δ_{LS} = 0.025 rad and δ_{CP} = 0.05 rad, at Immediate Occupancy (IO), Life Safety (LS) and Collapse Prevention (CP) limit states, respectively. The vertical dashed lines in the Figures represent these conventional drift capacities. The bold line indicates the median drift computed using the numerical data. In Figure 11, IDA curves for the "1991-3D" model are shown, those were obtained by means of direct integration of ground motion accelerograms, including P-Delta effects. The dash-dotted lines in Figure 11 represent the median and median plus/minus one standard deviation (of the logarithms) drift demand obtained by a linear regression of the logarithms of drifts over the logarithms of IMs. The dash-dot median line is very close, in the entire range of investigated IMs, to the response that would be obtained neglecting P-Delta effects from the numerical model, as well as, at levels of seismic intensity lower than 0.3 g, to the median obtained from the analyses. This implies that 0.3g is approximately the IM value starting from which the influence of P-Delta effects becomes significant. This result confirms what observed in SPO analysis (Fig. 10*b*).

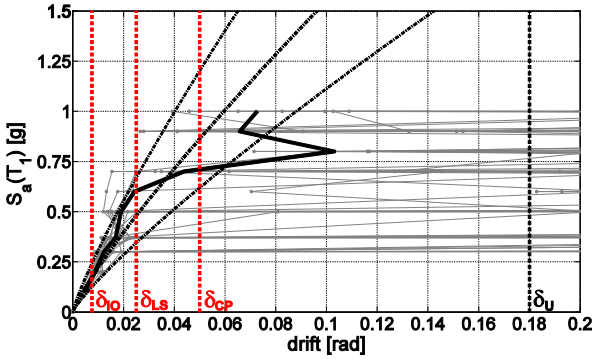

Figure 11. IDA results for "1991-3D" model.

Results from analysis of the "1991" 2D models are shown in Figure 12. Comparing the "1991-2D-Y" (Fig. 12*a*) with the 3D model results (Fig. 11*b*), it can be seen that the number of ground acceleration records leading to "instability" in case of the 3D model is larger than in case of the 2D model. This is a consequence of a larger slope for the degrading (post-peak) branch in the 3D model response. This larger sensitivity to the dynamic instability is partially compensated by the smaller value of the ultimate drift ratio obtained for the 2D model. Figure 12*b* shows that the IO limit state for frames in the *x*-direction is reached at spectral accelerations smaller than those in the *y*-direction. This is explained because of the larger flexibility of the *x*-direction structure. This latter gives also rise to larger sensitivity to P-Delta effects, what appears from the fact that a larger number of accelerograms produces drift demand larger than the ultimate value δ_U. The latter comment also explains why the bold line, that is the median of drift demand, indicates smaller drift demand, at a given large spectral acceleration value, when compared with the median in Figure 12*a*. In fact, drift values larger than δ_U were removed from the calculation of the median and treated separately as cases of certain collapse (see the companion paper for a discussion). Peak roof drift demand for the "1971-79" building is represented in Figure 13. When compared with results previously shown for other structures, it is possible to note that, in both the *y*-direction (Fig. 13*a*) and *x*-direction (Fig. 13*b*), the "1971/79" building is characterized by higher demand.

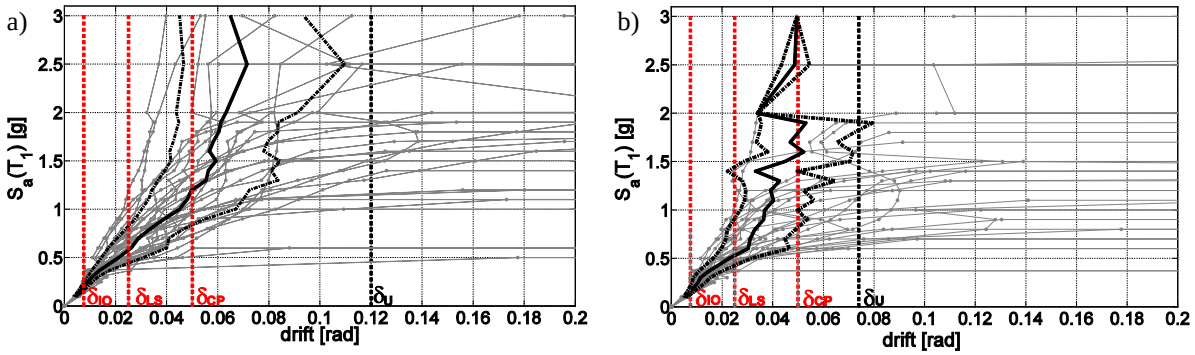

Figure 12. IDA results for "1991-2D-Y" (a) and "1991-2D-X" (b) models.

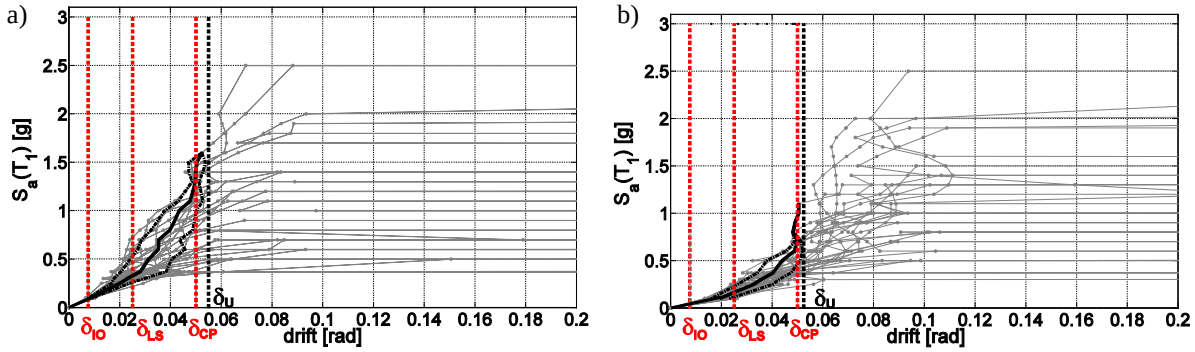

Figure 13. IDA results for "1971/79-2D-Y"(a) and "1971/79-2D-X" (b) models.

4.2.2. Local seismic demand and capacity (force)

Failure of any roof member and/or connections may pose serious problems of roof collapse, due to the statically determined structural scheme and the potentially brittle nature of these phenomena. As previously described, non-linear models do not include explicitly failure of roof elements and base plate welds. Therefore, the maximum force demand to roof elements and the maximum bending moment demand to column base plates have been computed from time history analyses. Figure 14 shows two samples of force demand on members belonging to the "1991-2D-Y" model.

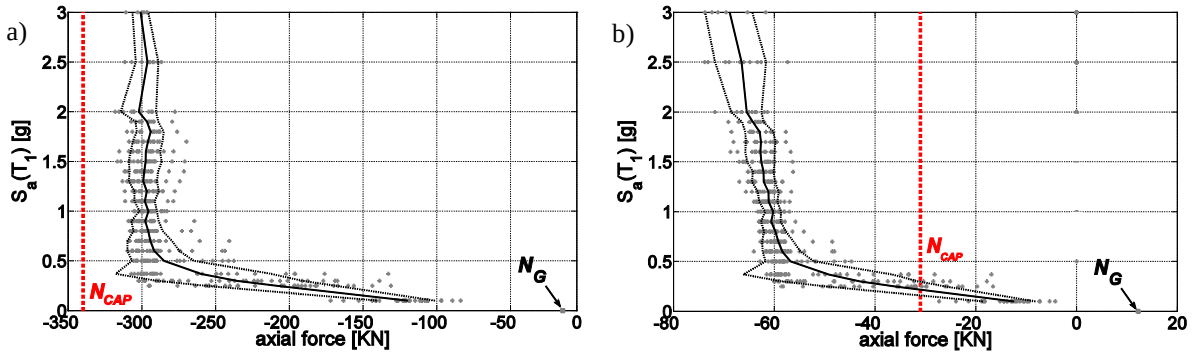

Figure 14. IDA results in terms of member force for two elements of "1991-2D-Y" model.

Starting from the value due to gravity loads (N_G), the axial force demand increases linearly (elastic response) at small levels of spectral acceleration. But when a plastic mechanism has been formed in the main frame (plastic hinges at bottom and top ends of each column), the axial force demand remains practically constant. Some variation in the force demand can still remain, because masses on the roof are distributed to also the top chord nodes and roof members are linear elastic. The vertical dashed line shown in the Figure 14 corresponds to the axial force capacity (N_{CAP}). Figure 14*a* refers to a member for which seismic demand never exceeds the capacity, while Figure 14*b* refers to a member,

originally subjected to compressive force due to gravity loads, which subsequently undergoes buckling failure due to earthquake loads. Many of such local failure modes were detected for the existing structures, thus highlighting the importance to monitor local force demand to those elements.

5. CONCLUSIONS

Seismic modelling and analysis of four existing industrial structures have been presented in the paper, the first part of a study whose discussion is completed in a companion paper dealing with probabilistic methodologies. One main difficulty of the analysis was the modelling of column base connections. Though experimental and/or finite element studies should rigorously be carried out, it has been shown that using the well-known components method (EC3), along with some reasonable assumptions, a plausible moment-rotation response can be obtained. Unfortunately, simple analysis methods to predict the rotation capacity and the hysteresis response are still not available. The importance to take into account failure of roof bracing elements has been highlighted by comparing results from two limit cases: (i) fully active bracing members and (ii) fully collapsed bracing members. Interestingly, the results highlight that the behaviour in case of fully active transverse bracing is not necessarily better than the behaviour of individual frames at large earthquake intensity, because of P-Delta effects generating a larger negative post-peak stiffness in the 3D model. Finally, the importance to include a careful analysis of peak force demand to roof elements was also highlighted. As a general outcome, the study highlighted the need of more research efforts addressed to produce guidelines for appropriate structural modelling of existing structures.

ACKNOWLEDGMENT

This work was partially supported by AXA-Matrix, within the AXA-DIST 2010-2013 research program, and partially by ReLUIS, within the ReLUIS-DPC 2010-2013 research program.

REFERENCES

ASCE American Society of Civil Engineers (2000). Pre-standard and Commentary for the Seismic Rehabilitation of Buildings (Report No. FEMA 356). Reston, VA: American Society of Civil Engineers prepared for the Federal Emergency Management Agency.

Brencich, A. (2010). Collapse of an industrial steel shed: A case study for basic errors in computational structural engineering and control procedures. *Engineering Failure Analysis* **17**, 213-225.

CEN , European Commitee for Standardization (2005). Eurocode 3: Design of steel structures – Part 1-8: Design of joints. PrUNI-EN 1993-1.8.

Della Corte, G., De Matteis, G., Landolfo, R. and Mazzolani, F.M. (2002). Seismic analysis of MR steel frames based on refined hysteretic models of connections.*Journal of Constructional Steel Research* **58**,1331-1345.

De Matteis, G., Landolfo, R., Mazzolani, F.M. (1999). Diaphragm effect for industrial steel buildings under earthquake loading. *Journal of Constructional Steel Research*, **46:1-3**, 357-358.

Dowell, R.K., Seible, F.S. and Wilson, E.L. (1998). Pivot hysteretic model for reinforced concrete members. *ACI Structural Journal* **95**, 607–617.

Ibarra, L.F., Medina, R.A. and Krawinkler, H. (2005). Hysteretic models that incorporate strength and stiffness deterioration. *Earthquake Engineering and Structural Dynamics* **34**, 1489-1511.

Mastrogiuseppe, S., Rogers, C.A., Tremblay, R., and Nedisan, C.D. (2008). Influence of nonstructural components on roof diaphragm stiffness and fundamental periods of single storey steel buildings. *Journal of Constructional Steel Research* **64**, 214227.

Ozakgul, K., Caglayan, O. and Tezer, O. (2011). Investigation of buckled brace system of an existing industrial building. *Engineering Failure Analysis* **18**, 455-463.

Petruzzelli, F., Iervolino, I. and Della Corte, G. (2012). Seismic Risk assessment of an industrial steel building, Part 2: fragility and failure probabilities. *15th World Conference on Earthquake Engineering*, Lisbon, Portugal.

Vamvatsikos, D. and Cornell, C.A. (2002). Incremental dynamic analysis. *Earthquake Engineering and Structural Dynamics* **31**, 491–514.

Wilson, EL. (2002) Three-dimensional static and dynamic analysis of structures. Berkeley (CA, USA). Computers & Structures, Inc.